Nano Research
2021, 14(11): 4173–4181
ISSN 1998-0124 CN 11-5974/O4
https://doi.org/10.1007/s12274-021-3359-2

Research Article

3D urchin like V-doped CoP *in situ* grown on nickel foam as bifunctional electrocatalyst for efficient overall water-splitting

Hongyao Xue[1], Alan Meng[2], Haiqin Zhang[3], Yusheng Lin[4], Zhenjiang Li[1,4] (✉), and Chuansheng Wang[5] (✉)

[1] *College of Electromechanical Engineering, Qingdao University of Science and Technology, Qingdao 266061, China*
[2] *Key Laboratory of Optic-electric Sensing and Analytical Chemistry for Life Science, MOE, College of Chemistry and Molecular Engineering, Qingdao University of Science and Technology, Qingdao 266042, China*
[3] *Shandong Shida Shenghua Chemical Group Co., Ltd., Dongying 257503, China*
[4] *College of Materials Science and Engineering, Qingdao University of Science and Technology, Qingdao 266061, China*
[5] *National Engineering Laboratory for Advanced Equipments and Key Materials for Tires, Qingdao University of Science and Technology, Qingdao 266042, China*

Received: 15 November 2020 / **Revised:** 31 December 2020 / **Accepted:** 24 January 2021

ABSTRACT

Cobalt phosphide (CoP) is considered to be a potential candidate in the field of electrocatalysis due to its low-cost, abundant resources and high electrochemical stability. However, there is a great space for further improvement of its electrocatalytic performance since its charge transfer rate and catalytic activity have not reached a satisfactory level. Herein, we design and fabricate a three dimensional urchins like V-doped CoP with different amounts of V-doping on nickel foam electrode. The V-doped CoP/NF electrode with optimized amounts of V-doping (10%) exhibits outstanding hydrogen evolution reaction (HER) performance under universal-pH conditions and preeminent oxygen evolution reaction (OER) performance in alkaline media. Notably, the assembled water-splitting cell displays a cell voltage of only 1.53 V at 10 mA·cm^{-2} and has excellent durability, much better than many reported related bifunctional catalysts. The experiment results and theoretical analysis revealed that vanadium atoms replace cobalt atoms in CoP lattice. Vanadium doping can not only raise the density of electronic states near the Fermi level enhancing the conductivity of the catalyst, but can also optimize the free energy of hydrogen and oxygen-containing intermediates adsorption over CoP, thus promoting its catalytic activity. Moreover, the unique nanostructure of the catalyst provides the various shortened channels for charge transfer and reactant/electrolyte diffusion, which accelerates the electrocatalytic process. Also, the *in situ* growth strategy can improve the conductivity and stability of the catalyst.

KEYWORDS

overall water-splitting, V-doping, urchins like, density functional theory (DFT), density of states (DOS)

1 Introduction

With the development of fuel vehicles, the climax of building hydrogen refueling stations is emerging all over the world, so it is necessary to find a safe and efficient technology to produce hydrogen [1, 2]. In large-scale hydrogen production, compared with the traditional coal gasification method and steam-methane reforming method, electrochemical water-splitting method has attracted more attention because it is environmental-friendly, renewable and has convenient preparation process [3, 4]. To realize high performance electrolytic water-splitting composed of two half-reactions of hydrogen evolution reaction (HER) and oxygen evolution reaction (OER), Pt and Ru/Ir-based materials are considered as the state-of-the-art electrocatalysts for HER and OER, respectively [5]. However, their scarcity and high cost make them unsuitable for large-scale applications [6–8]. Finding alternative electrocatalyst that are inexpensive with better stability and high catalytic activity has become an indispensable topic in the application of extensive electrochemical water-splitting [9].

In recent years, cobalt phosphide (CoP) has been regarded as a potential material in the field of electrocatalysis because of its low-cost, earth abundance and high electrochemical stability [10, 11]. However, the electrocatalytic performances of CoP are still far from satisfying the requirements of practical application due to its relatively slow charge transfer rate and low electrochemical activity [12]. Therefore, current studies mainly focus on how to improve the electrocatalytic performance of CoP. Based on previous reports, introducing metal element into CoP is considered to be an effective way to adjust its electronic structure and optimize its electronic conductivity in order to improve its electrocatalytic performance [13–16]. For instance, Al-doped CoP [13] and Mn-doped CoP [14] were reported, to show attractive electrochemical performance. In another work reported by Ho et al., Ce-doped CoP as HER catalyst, exhibited outstanding performance compared to pristine CoP [15]. Consequently, introducing metal elements into CoP has been considered as a key factor to boost its electrochemical water-splitting performance. In particular, vanadium was a satisfactory candidate due to its low cost, abundant resources and the closeness of its atomic radius to that of cobalt. Another efficient way that can be used to enhance the catalytic ability

Address correspondence to Zhenjiang Li, zhenjiangli@qust.edu.cn; Chuansheng Wang, wcsmta@qust.edu.cn

of CoP is its nanostructure design [17, 18]. Recently, CoP nanoneedle arrays grown on carbon cloth [19], CoP nanoframes [20], and hierarchical ultrathin CoP nanosheets [21] were fabricated. It was proven, that CoP with specific morphology had improvement in its overall water splitting performance. By comparison with powder catalytic materials, the direct growth of catalysts on substrates, can provide more exposed active sites, reduce contact resistance and promote the stability of electrodes [22]. For example, Hou and co-workers synthesized NC–NiCu–NiCuN electrode with a high catalytic activity by *in situ* growth strategy [23]. CoP microscale prism-like superstructure arrays on Ni foam [24] and as-prepared Co/CoP film on Ni foam [25] as efficient-electrocatalyst manifested robust catalytic activity. Hence, the *in situ* growth strategy also helped to improve the electrochemical performance of CoP.

In this work, we combined the above effective strategies to prepare a three-dimensional (3D) urchin like V-doped CoP nanostructure *in situ* grown on commercially available nickel foam through a hydrothermal–phosphidation method. When the optimized amount of doping is 10%, the V-doped CoP/NF electrode showed excellent catalytic performance toward HER and OER. From the experiments and theoretical calculations, the substitution of vanadium for cobalt in CoP had a significant influence on the catalytic performances of CoP. The density functional theory (DFT) calculations suggest that vanadium doping leads to optimal free energies of hydrogen and oxygen-containing intermediates adsorption. Density of states (DOS) result demonstrates that V-doping can enhance the conductivity of CoP during the electrocatalytic process by regulating its surface electronic state. Moreover, its unique nanostructure provided various shortened channels for charge transfer and reactant/electrolyte diffusion, thereby accelerating the electrochemical reaction process; also the *in situ* growth strategy facilitated the intimate contact between the catalytic materials and nickel foam, thus maximizing the electrical conductivity and stability of the electrode. Therefore, the as-prepared electrode has a broad application prospect in the field of electrocatalysis because of its impressive catalytic performance in water-splitting.

2 Experimental

2.1 Preparation of Ni foam

A piece of Ni foam (1.2 cm ×1.2 cm) was soaked in 2.0 mol HCl for 10 min to remove the NiO on the surface. It was washed with ethanol and deionized water, respectively, and then dried at room temperature.

2.2 Synthesis of V-Co(OH)F/NF precursor

In a typical synthesis, 3 mmol $Co(NO_3)_2{\cdot}6H_2O$, 0.3 mmol VCl_3, 15 mmol $CO(NH_2)_2$ and 9 mmol of NH_4F were added to a solution of 150 mL deionized water and stirred continuously. The homogenous mixture and a piece of Ni foam were transferred to Teflon-lined stainless steel autoclave, which was then sealed and kept in the oven at 120 °C for 8 h. The autoclave was cooled down to room temperature and the V-Co(OH)F/NF was then washed with ethanol and deionized water, respectively, and dried at room temperature.

2.3 Synthesis of V-doped CoP/NF

The as-prepared precursor V-$Co(OH)_2$/NF and NaH_2PO_2 powder (6 times in mass) was put in two separate positions in a ceramic boat with NaH_2PO_2 at the upstream side of the tube furnace. After annealing the sample at 350 °C for 2 h and at a heating rate of 3 °C·min^{-1} under Ar atmosphere, V-doped CoP/NF was obtained.

2.4 Comparison of samples

The corresponding electrodes with different vanadium doping contents were synthesized, and denoted as CoP/NF, V_5-doped CoP/NF and V_{15}-doped CoP (5, 15 represent the molar percent of vanadium added to CoP in the starting material).

3 Results and discussion

The synthesis procedure of 3D urchin like V-doped CoP nanostructure on nickel foam is shown in Scheme 1. Firstly, VCo-OH-F/NF precursor with urchin like morphological features was prepared by hydrothermal method. It was formed by high density of aligned nanoneedle arrays with length of about 1 μm, and its uniform size distribution is about 3–5 μm. Then, it was converted into V-doped CoP/NF after a simple annealing process in the presence of NaH_2PO_2 and its morphology basically retained the original characters of its hydroxide counterparts.

The scanning electron microscopy (SEM) technique was employed to explore the surface morphology and microstructure of the catalyst. The SEM images of the as-fabricated precursor (VCo-OH-F/NF) with optimized V-doping amount (10%) are shown in Fig. S1 in the Electronic Supplementary Material (ESM). Figures 1(a)–1(c) showed SEM images of the V-doped CoP/NF electrode obtained by phosphating process. It shows the formation of spherical urchin like nanostructure with diameter of about 3–5 μm, and is composed of numerous small nanoneedles radially grown from the center. In Figs. S2–S4 in the ESM, the V-doping content had no significant influence on the urchin like nanostructure morphology, but it affected the average grain size of the catalysts. It can be clearly seen that the size of urchin-like nanostructure decreased with increase in the

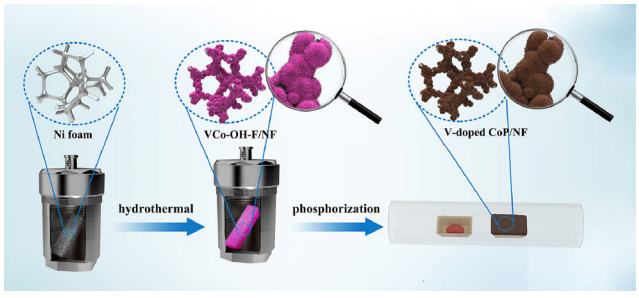

Scheme 1 Schematic illustration of synthetic routes of urchins like V-doped CoP/NF.

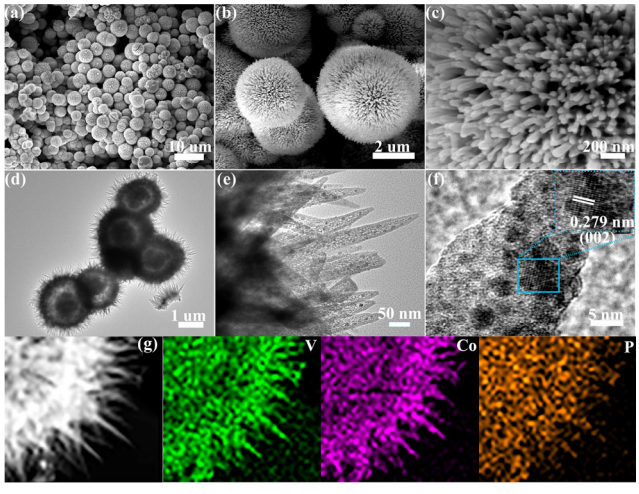

Figure 1 (a)–(c) SEM images of V-doped CoP/NF. (d) and (e) TEM images of V-doped CoP. (f) HR-TEM image of V-doped CoP. (g) TEM image and element mapping of V, Co and P.

amount of V doping. It could be that the reduction of the relative content of cobalt hindered the growth of the nanostructure. To further understand the microstructural characteristics of the materials, transmission electron microscopy (TEM) and high-resolution TEM (HR-TEM) were carried out. The TEM images of the precursor with optimized V-doping amount are shown in Fig. S5 in the ESM, which coincided with the above SEM result. As can be seen in Figs. 1(d) and 1(e), the TEM images further suggested that the urchin like nanostructure contained numerous tiny nanoneedles with diameter of approximately 30–40 nm, which provided a large contact area with the electrolyte and shortened ion/electron transport pathways. The HR-TEM image taken from a V-doped CoP nanoneedle is shown in Fig. 1(f), and the clearly resolved lattice fringes were calculated to be roughly 0.279 nm, corresponding to the (002) plane of spinel structured CoP. Energy dispersive X-ray spectroscopy (EDX) elemental mapping images (Fig. 1(g)) indicate that vanadium, cobalt and phosphorus elements are uniformly distributed, which demonstrated the successful introduction of V atom into CoP.

The phase composition of the pristine CoP and V-doped CoP was confirmed by X-ray diffraction (XRD) characterization (Fig. 2(a)). Without V-doping, all the Bragg peaks observed corresponded to the hexagonal phase of pristine CoP (JCPDS card No. 29-0497). The XRD pattern of the as-obtained V-doped CoP with optimized doping amount (10%) was similar to that of pristine CoP, and there was no detectable new diffraction peak. As shown in the inset of Fig. 2(a), the (211) diffraction angle of V-doped CoP slightly shifted to lower position, which may result from reduction of lattice parameters caused by V-doping in CoP. As shown in Fig. S6 in the ESM, when V-doping amounts increased to 15%, V_{15}-doped CoP showed new peak at about 40°, which can be easily indexed to V_2P (JCPDS card No. 65-2394).

X-ray photoelectron spectroscopy (XPS) measurement was carried out to investigate the detailed elemental compositions and valence states of V-doped CoP. In Fig. S7 in the ESM, the characteristic peaks of Co, V and P could be clearly observed, and the appearance of O might be due to the partial oxidation of the sample during the drying step and the post-treatment process. The high-resolution Co 2p spectrum displayed two doublets associated with Co $2p_{3/2}$ and Co $2p_{1/2}$ characteristics, as well as two shakeup satellite peaks at 786.7 and 803.2 eV, respectively (Fig. 2(b)). In this context, two peaks located at 778.9 and 793.5 eV corresponded to the Co–P bond [26]. Besides, another two peaks located at 782.1 and 797.9 eV were on account of the oxidized state of Co from Co-phosphate [27, 28]. The two peaks of the P 2p spectrum at a binding energy of 129.7 and 130.3 eV were assigned to the P $2p_{3/2}$ and P $2p_{1/2}$ regions of the V-doped CoP/NF, respectively, and the peak at 133.9 eV indicated the formation of oxidized phosphate on the surface of the nanostructures (Fig. 2(c)), because the sample came into contact with air during the processing. The V 2p XPS spectrum of V-doped CoP/NF in Fig. 2(d) can be decomposed into V $2p_{3/2}$ and V $2p_{1/2}$ at 516.8 and 524.2 eV, respectively. In particular, the two peaks at the binding energy of 516.2 and 523.5 were attributed to V^{3+}, confirming the formation of V–P bond. This shows that vanadium element was successfully introduced into the crystal lattice of CoP. The two peaks at 517.1 and 524.4 eV were assigned to V^{4+} and another two peaks at 517.9 and 525.3 eV corresponded to V^{5+}, which belonged to V–O bond. The results indicate that V^{3+} was partially oxidized to V^{4+} and V^{5+} during the synthesis [29]. The analysis of SEM, TEM images, XRD and XPS spectra confirmed that the V-doped CoP catalyst was successfully synthesized.

To investigate the effect of vanadium doping content on the electrocatalytic properties of the catalyst, the HER performance of V-doped CoP/NF with different vanadium content was evaluated using a standard three-electrode system in 1 M KOH at a scan rate of 5 $mV \cdot s^{-1}$ with 90% *iR*-compensation (details in the ESM). As we know, doping can tune the free energy (ΔG_{H^*}) of H adsorption on the surface of catalyst, which is a key descriptor used to predict the activity of catalysts. The value of ΔG_{H^*} is strongly decided by the amount of dopant. A too large or small value of ΔG_{H^*} indicates a very strong or weak interaction between the active sites and the

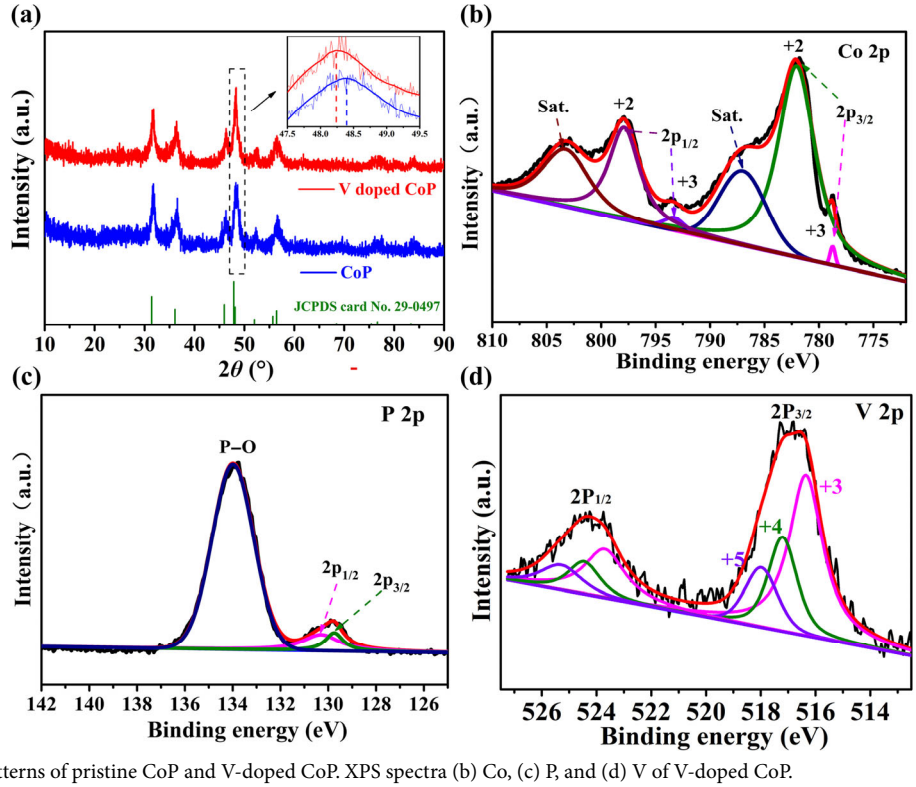

Figure 2 (a) XRD patterns of pristine CoP and V-doped CoP. XPS spectra (b) Co, (c) P, and (d) V of V-doped CoP.

intermediates, which is not beneficial for the HER [30]. Figure 3(a) showed the HER performance of the electrode materials with 0%, 5%, 10% and 15% vanadium content, respectively. When the vanadium content was 10%, the material had the best HER performance (overpotential of 84.6 mV at 10 mA·cm^{-2}), indicating that an appropriate V-doping content could improve the catalytic performance of the catalyst. An electrochemical test was carried out under the optimal vanadium content. Also, VCo-OH-F/NF, CoP/NF, Ni foam and Pt/C were used as control samples. Figure 3(b) display the linear sweep voltammetry (LSV) curves in 1 M KOH solution. The required overpotential of V-doped CoP/NF (84.6 mV) was very close to that of Pt/C (70 mV) at a current density of 10 mA·cm^{-2}, outperforming those of VCo-OH-F/NF (173.5 mV), CoP/NF (141.2 mV) and Ni foam (265 mV). The overpotential of the catalyst was much better than that of the other Co-based phosphide catalysts in previous reports (see Table S1 in the ESM). To gain insight into the catalytic HER behaviour of the catalyst in terms of the electron/mass transport and reaction kinetic, the corresponding Tafel slopes were calculated according to LSV curves. As shown in Fig. 3(c), the V-doped CoP/NF showed a Tafel-slope of 79.2 mV·dec^{-1}, which was smaller than those of VCo-OH-F/NF, CoP/NF and Ni foam (100.7, 86.4 and 182.9 mV·dec^{-1}, respectively). Besides the HER activity, stability is another important indicator to evaluate an advanced electrocatalyst. As shown in Fig. 3(d), the LSV curves after the

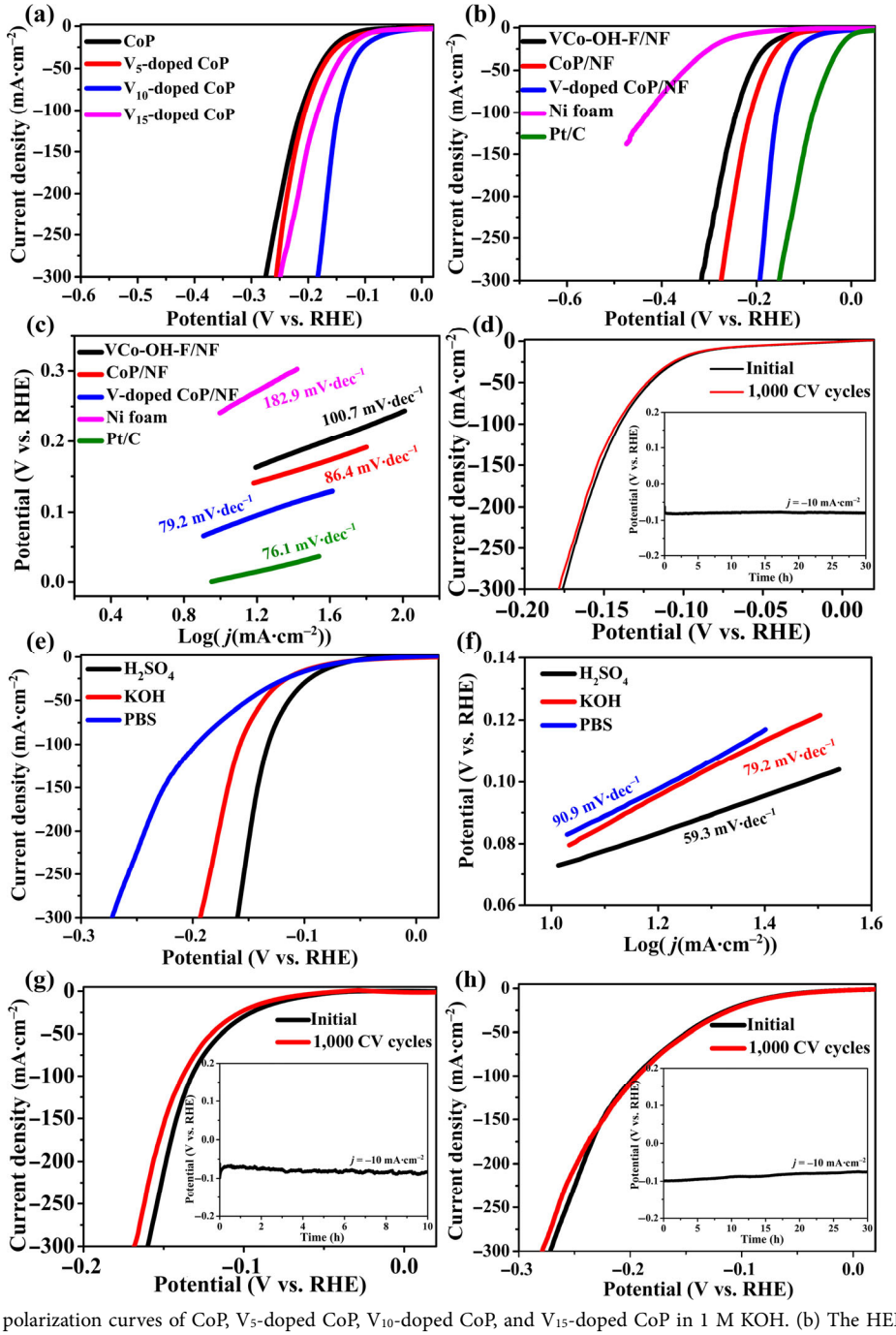

Figure 3 (a) The HER polarization curves of CoP, V_5-doped CoP, V_{10}-doped CoP, and V_{15}-doped CoP in 1 M KOH. (b) The HER polarization curves of VCo-OH-F/NF, CoP/NF, V-doped CoP/NF, Ni foam and Pt/C in 1M KOH and (c) corresponding Tafel plots of VCo-OH-F/NF, CoP/NF, V-doped CoP/NF, Ni foam and Pt/C. (d) HER durability measurement of V-doped CoP/NF and polarization curves of V-doped CoP/NF before and after 1,000 CV cycles. (e) The HER Polarization curves of V-doped CoP/NF in 0.5 M H_2SO_4, 1 M KOH and 1 M PBS and (f) corresponding Tafel plots V-doped CoP/NF in 0.5 M H_2SO_4, 1 M KOH and 1 M PBS. (g) HER durability measurement of V-doped CoP/NF in 0.5 M H_2SO_4 and polarization curves of V-doped CoP/NF before and after 1,000 CV cycles. (h) HER durability measurement of V-doped CoP/NF in 1 M PBS and polarization curves of V-doped CoP/NF before and after 1,000 CV cycles.

CV experiment exhibited a negligible loss in current density compared to the initial one. The inset in Fig. 3(d) presented that it possessed a superior stability with negligible potential degradation at 10 mA·cm^{-2} for 30 h by chronopotentiometry (CP) measurements.

Figure 3(e) illustrates the LSV curves of V-doped CoP/NF in 0.5 M H_2SO_4, 1 M PBS and 1 M KOH, which was used to evaluate the HER performance of the materials in a wide pH range. It can be seen that the V-doped CoP/NF had the best HER performance under acidic conditions (0.5 M H_2SO_4). Its overpotential values were 73 and 133 mV at current density of 10 and 100 mA·cm^{-2}, respectively, and the Tafel slope was 59.3 mV·dec^{-1} (Fig. 3(f)). V-doped CoP/NF showed a long-term stable performance after 1,000 CV sweeps in 0.5 M H_2SO_4 (Fig. 3(g)). Furthermore, when a current density of 10 mA·cm^{-2} was applied for 10 h, only a slight increase in the required overpotential could be observed (Fig. 3(g) inset). In addition, considering the corrosion of acid solution to the electrode, an ICP test was carried out to further explore its stability. The ICP test results (see Table S2 in the ESM) presented that Ni content of V-doped CoP/NF in H_2SO_4 solution was much lower than that of pristine NF. This indicates that catalyst *in situ* grown uniformly on the surface of NF can effectively protect the NF from corrosion by H_2SO_4 electrolytes, thus improving the stability of the electrode. Under neutral pH of environmental solutions, the overpotentials were 86 and 197 mV at current density of 10 and 100 mA·cm^{-2}, respectively, and the Tafel slope was 90.9 mV·dec^{-1}. In order to test its durability in 1 M PBS, the LSV curve was recorded again after 1,000 cycles. Compared to the original one, no remarkable difference could be seen (Fig. 3(h)). Furthermore, when a current density of 10 mA·cm^{-2} was applied for 30 h, only a slight increase in the required overpotential could be observed (Fig. 3(h) inset). These above results demonstrated that V-doped CoP/NF electrode had high catalytic activity and stability in a wide pH range, which provided a beneficial reference for the practical application of electrocatalytic materials in the future.

The OER performances of the catalysts were investigated in N_2-saturated alkaline media (1 M KOH). As shown in Fig. 4(a), the required overpotential of V-doped CoP/NF was only 265.3 mV at a current density of 20 mA·cm^{-2}, which was superior to that of VCo-OH-F/NF (289.4 mV), CoP/NF (326 mV), Ni foam (371.4 mV), RuO_2 (328 mV) as well as many other Co-based phosphide catalysts (see Table S3 in the ESM). As shown in Fig. 4(b), the superior OER performance of the V-doped CoP/NF was also confirmed by its extremely low Tafel-slope (66.2 mV·dec^{-1}) derived from LSVs, which was much smaller than those of VCo-OH-F/NF (71.1 mV·dec^{-1}), CoP/NF (150.6 mV·dec^{-1}), Ni foam (268.5 mV·dec^{-1}) and RuO_2 (106.2 mV·dec^{-1}). In addition, the LSV changes of V-doped CoP/NF before and after 1,000 sweeps are shown in Fig. 4(c), and the almost overlapping LSV curves demonstrated the long-term OER stability of V-doped CoP/NF. This excellent durability is also supported in the inset of Fig. 4(c), in which only a trifling increase of potential was observed after 30 h of continuous OER electrolysis in 1 M KOH. The reason for the outstanding stability of the electrode can be attributed to the *in situ* growth strategy, which provided intimate electrical contact between the catalytic material and the current collector, preventing the catalyst from falling off casually. An electrochemical impedance spectroscopy (EIS) experiment was performed to explore the charge transfer properties. Figure 4(d) demonstrates that the V-doped CoP/NF electrode generated smaller semicircle radii than VCo-OH-F/NF and CoP/NF electrodes, indicating its excellent efficient electronic transmission in the electrocatalytic process. The improved conductivity of V-doped CoP was explicated as follows: In pristine CoP crystal, outermost shell electrons of Co and P atoms were constrained by covalent bonds. Only very few amount of electrons became free carrier due to thermal excitation at room temperature. In other word, the conductivity of pristine CoP was poor. After V doping into CoP, V atoms replaced the position of partial Co atoms. Since the coordination number of V was larger than that of Co, the extra free electrons moved directionally under the applied electric field, contributing to a higher conductivity than pristine CoP.

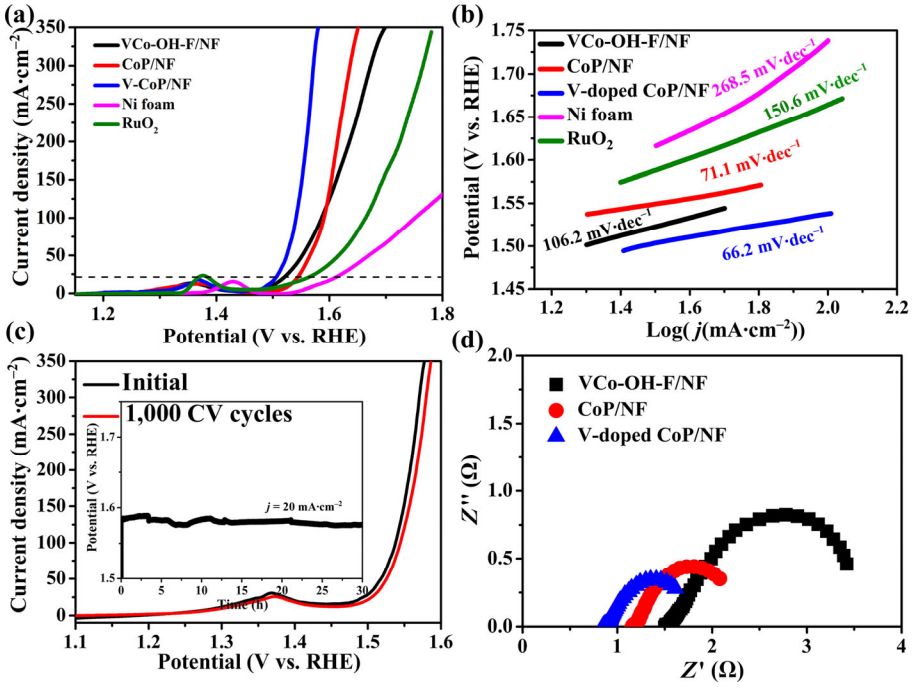

Figure 4 (a) The OER polarization curves of VCo-OH-F/NF, CoP/NF, V-doped CoP/NF, Ni foam and RuO_2 in 1M KOH and (b) corresponding Tafel plots of VCo-OH-F/NF, CoP/NF, V-doped CoP/NF, Ni foam and RuO_2. (c) OER durability measurement of V-doped CoP/NF and polarization curves of V-doped CoP/NF before and after 1,000 CV cycles. (d) Nyquist plots of VCo-OH-F/NF, CoP/NF and V-doped CoP/NF.

We can evaluate the intrinsic catalytic activity of the materials by comparing the calculated value of turnover frequency (TOF). In the first step, the double-layer capacitance (C_{dl}) is evaluated by a series of cyclic voltammetry (CV) measurements at 10 to 60 mV·s^{-1} scan rates. Next, we can calculate the electrochemical active surface area (ECSA). Finally, the TOF value is estimated according to the determination of ECSA (The calculation details are presented in the ESM). As can be seen in Fig. 5(a) and Fig. S8 in the ESM, C_{dl} of V-doped CoP/NF (54.7 mF·cm^{-2}) was much higher than that of VCo-OH-F/NF (9.1 mF·cm^{-2}), CoP/NF (21 mF·cm^{-2}) and Ni foam (1.5 mF·cm^{-2}). In addition, V-doped CoP/NF possessed a great ECSA of 1,367.5 cm^2, which was much larger than that of VCo-OH-F/NF (525 cm^2), CoP/NF (227.5 cm^2) and Ni foam (37.5 cm^2), respectively (Fig. 5(b)).

The intrinsic catalytic activities of the V-doped CoP/NF were determined by TOF value. As shown in Fig. 5(c), the TOF_{HER} at η = 300 mV of V-doped CoP/NF (2.8 S^{-1}) was higher than that of VCo-OH-F/NF (1.05 S^{-1}), CoP/NF (1.75 S^{-1}) and Ni foam (0.03 S^{-1}), respectively. The TOF_{OER} at η = 350 mV of V-doped CoP/NF (1.8 S^{-1}) was higher than that of VCo-OH-F/NF (0.35 S^{-1}), CoP/NF (0.28 S^{-1}) and Ni foam (0.11 S^{-1}), respectively (Fig. 5(d)). The above results suggest the maximum exposure level of the effective active sites on the three dimensional urchins like V-doped CoP/NF electrode was beneficial to adsorption and dissociation of water molecules. It also provided easy contact with the electrolyte, thereby significantly enhancing the catalytic activity of the catalyst.

In order to assess the promising large-scale application of the bifunctional V-doped CoP/NF for water splitting, V-doped CoP/NF was further used as anode and cathode simultaneously in a cell. Figure 5(e) shows that V-doped CoP/NF//V-doped CoP/NF displayed a high electrocatalytic activity with a cell voltage of 1.53 V to reach a current density of 10 mA·cm^{-2}, which is superior to many other reported overall water-splitting systems (see Table S4 in the ESM); Pt/C//RuO_2 also had a high electrocatalytic activity with a cell voltage of 1.57 V. This reveals the prominent performances of the catalysts. The chronopotentiometry test was carried out for 160 h at 10 mA·cm^{-2} for overall water-splitting (Fig. 5(f)). The results show that the cell maintains a nearly constant potential for a very long time, indicating that V-doped CoP/NF electrode has an impressive durability.

In order to explore the underlying reason for the enhanced electrocatalytic activity of V-doped CoP, DFT calculation was done to investigate the effect of V-doping. To determine the V-doping site, three calculated models of V-doped CoP monolayer were established, which included V substituted Co sites, V substituted P sites and V doped in hole sites, respectively (Fig. S9 in the ESM). The corresponding formation energies of

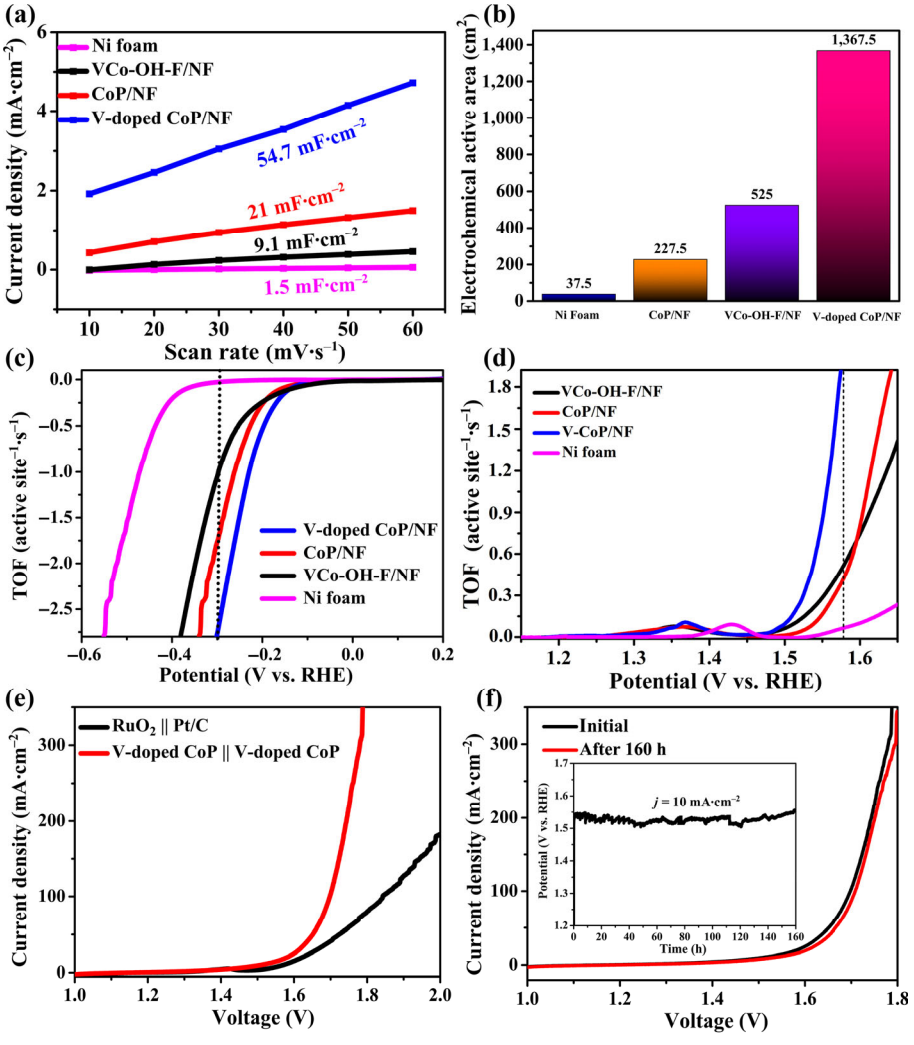

Figure 5 (a) C_{dl} values of VCo-OH-F/NF, CoP/NF, V-doped CoP/NF and Ni foam. (b) ECSA spectra for VCo-OH-F/NF, CoP/NF, V-doped CoP/NF and Ni foam. (c) TOF for HER. (d) TOF for OER. (e) Polarization curves of water electrolysis for V-doped CoP/NF//V-doped CoP/NF and Pt/C//RuO_2 with a scan rate of 5 mV·s^{-1} in 1.0 M KOH. (f) Polarization curves of V-doped CoP/NF before and after 160 h (inset, chronoamperometry curve of V-doped CoP/NF at 10 mA·cm^{-2} for 160 h).

these cases were 2.03, 2.36, and 8.07 eV, respectively, indicating that V dopants were liable to substitute the Co sites.

The calculation result was consistent with the experimental results, demonstrating that V substituted Co sites in CoP lattice. Figures 6(a) and 6(b) displayed atomic structures of pristine CoP and V-doped CoP, respectively. Because the HER activity was affected by the adsorption/desorption energetics of H* on the electrocatalyst, the adsorption free energy of hydrogen (ΔG_{H^*}) was used to assess the HER activity [31–33]. Obviously, after structural optimization, for pristine CoP, H* was preferentially adsorbed on metal Co, while for V-doped CoP, H* was preferentially adsorbed on metal V (Figs. S10 and S11 in the ESM). As can be seen in Fig. 6(c), compared to pristine CoP (0.73 eV), V-doped CoP possessed a lower ΔG_{H^*} value (0.29 eV), which was closer to the optimal ΔG_{H^*} (0 eV). This indicates that the V-doped CoP had a lower reaction barrier compared to the pristine CoP. This shows that the V-doping could improve the HER performance of the catalyst effectively. Next, we focused on the origin of the high OER activity of the V-doped CoP. As shown in Fig. 6(d) and Figs. S12 and S13 in the ESM, the free energy diagrams of the OER processes consist of typical four elementary steps under alkaline condition ($4OH^- \rightarrow 2H_2O + O_2 + 4e^-$)

(1) $HO^- + * \rightarrow HO^* + e^-$

(2) $HO^* + HO^- \rightarrow O^* + H_2O + e^-$

(3) $O^* + HO^- \rightarrow HOO^* + e^-$

(4) $HOO^* + HO^- \rightarrow * + O_2 + H_2O + e^-$

Among the four elementary steps, the step showing the largest free energy difference was the potential determining step (PDS) during the OER process [34, 35]. Accordingly, the PDS for V-doped CoP was determined to be the second step ($HO^* \rightarrow O^*$), and the ΔG_2 and corresponding calculated overpotential η were calculated to be 2.13 and 0.9 V, which were much smaller than that of pristine CoP (ΔG_2 = 2.3 eV, η = 1.07 V). The above calculations demonstrated that V-doping significantly strengthened the OER activity of CoP. As shown in Figs. 6(e) and 6(f), the electronic state of V-doped CoP close to the Fermi level was apparently higher than that of CoP, which shows that more charge carriers can be introduced via V-doping, to increase the conductivity of CoP. Especially, the DOS plots showed that conducting charges were observed on P, Co and V elements, and the orbital hybridization of three elements at the Fermi level promoted fast charge transfer during the electrocatalytic process.

The origin of the excellent performance of the V-doped CoP/NF electrode can be mainly attributed to the following:

(1) Unique 3D urchins like architecture with high density of aligned nanoneedle arrays offered abundant exposed catalytic reaction sites. This enabled the storage of electrolyte, which in turn facilitated electron/mass transfer during the HER and

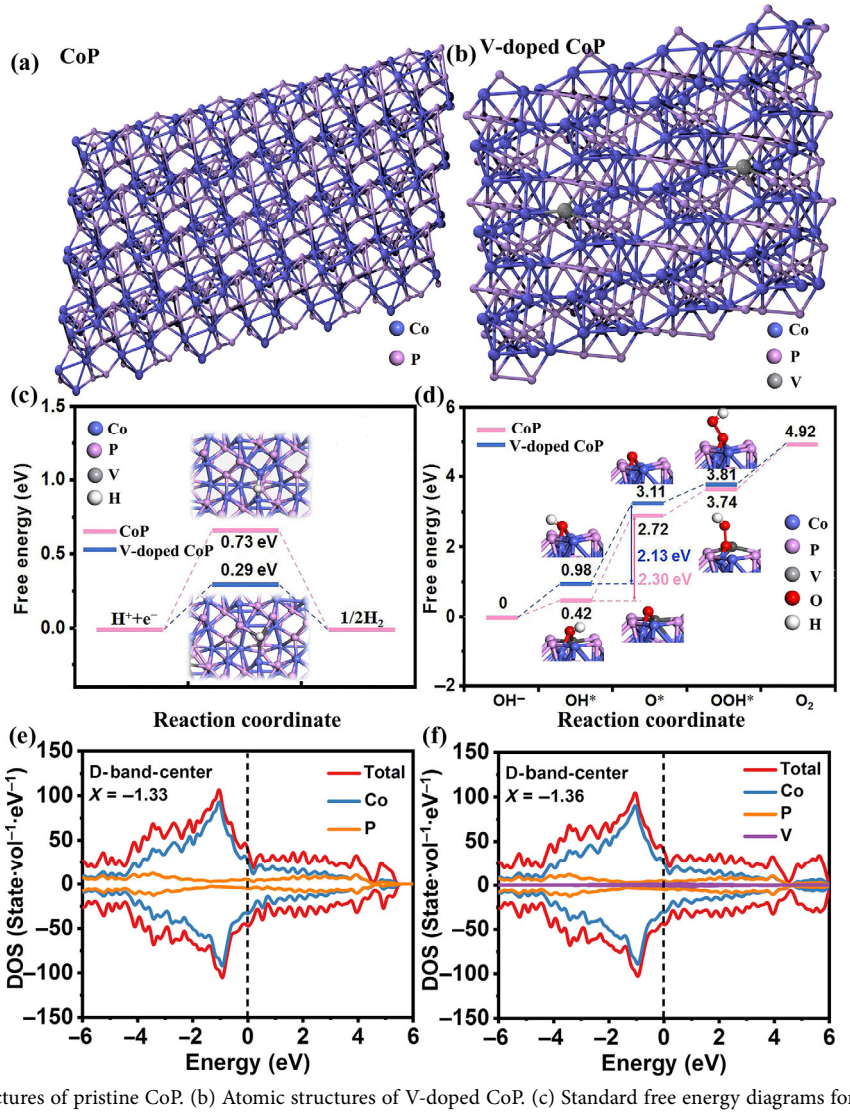

Figure 6 (a) Atomic structures of pristine CoP. (b) Atomic structures of V-doped CoP. (c) Standard free energy diagrams for the HER on pristine CoP and V-doped CoP. (d) Standard free energy diagrams for the OER on pristine CoP and V-doped CoP and the corresponding primitive steps. DOS (Fermi level is set to zero) for pristine CoP (e) and V-doped CoP (f).

OER activities.

(2) The catalyst had high bonding strength with Ni foam substrate by *in situ* growth strategy, which can reduce interface resistance and enhance electrical conductivity of electrode.

(3) Catalyst *in situ* grown uniformly on the surface of Ni foam can effectively protect the Ni foam from corrosion in solution, thus improving the stability of the electrode.

(4) The V atoms introduced optimized the adsorption free energy of hydrogen and oxygen-containing intermediates, which led to the enhanced kinetics for water splitting.

(5) The lower coordinated V sites substantially elevated the electronic activity, which facilitated the surface electronic exchange-and-transfer capabilities.

4 Conclusion

In summary, we introduced an effective hydrothermal and low-temperature phosphidation method to synthesize V-doped CoP *in situ* grown on Ni foam electrode with optimized doping amount, which possessed superior HER and OER performance (overpotential for HER: 84.6, 73, 86 mV at 10 mA·cm^{-2} in alkaline, acidic, and neutral electrolytes; overpotential for OER: 265.3 mV at 20 mA·cm^{-2} in basic media). Compared with devices based on Pt/C and RuO_2, the water-splitting cell of V-doped CoP/NF exhibited smaller cell voltage of 1.53 V at 10 mA·cm^{-2}. By calculating and comparing the formation energies of different V-doping models, we firstly determined that V atoms substitute for Co rather than P in the CoP model. The DFT results showed that the value of ΔG_{H^*} on the V-doped CoP is 0.29 eV, smaller than that of pristine CoP (0.73 eV), and correspondingly, the value of ΔG for OER on the V-doped CoP is 2.13 eV, lower than that of pristine CoP (2.3 eV). The above calculations suggest that V substitution leads to more optimal free energy of hydrogen and oxygen-containing intermediates adsorption. In addition, the DOS near fermin level was more intense than that of pristine CoP, which implied an enhanced charge concentration and electrical conductivity via V-doping. The unique urchin like nanostructure not only increased the number of exposed active sites, but also accelerated the reactants/electrolytes diffusion, thus speeding up the catalytic reaction process. The intimate contact between the catalytic materials and substrate derived from *in situ* growth strategy further maximize the electrical conductivity and stability of the electrode. This work afforded a guiding strategy for the synthesis of an eminent bifunctional electrocatalyst.

Acknowledgements

The work reported here was supported by the National Natural Science Foundation of China (No. 52072196). We acknowledge the National Supercomputing Center in Shenzhen, P. R. China for their computations assistance.

Electronic Supplementary Material: Supplementary material (e.g., SEM measurements, TEM measurements, the optimized geometry of H_2 and O_2 intermediates adsorption measurements) is available in the online version of this article at https://doi.org/10.1007/s12274-021-3359-2.

References

[1] Wu, Y. W.; Wang, H.; Ji, S.; Pollet, B. G.; Wang, X. Y.; Wang, R. F. Engineered porous Ni_2P-nanoparticle/Ni_2P-nanosheet arrays via the Kirkendall effect and Ostwald ripening towards efficient overall water splitting. *Nano Res*. **2020**, *13*, 2098–2105.

[2] Tang, W. K.; Liu, X. F.; Li, Y.; Pu, Y. H.; Lu, Y.; Song, Z. M.; Wang, Q.; Yu, R. H.; Shui, J. L. Boosting electrocatalytic water splitting via metal-metalloid combined modulation in quaternary Ni-Fe-P-B amorphous compound. *Nano Res*. **2020**, *13*, 447–454.

[3] Staszak-Jirkovsky, J.; Malliakas, C. D.; Lopes, P. P.; Danilovic, N.; Kota, S. S.; Chang, K. C.; Genorio, B.; Strmcnik, D.; Stamenkovic, V. R.; Kanatzidis, M. G. et al. Design of active and stable Co–Mo–S_x chalcogels as pH-universal catalysts for the hydrogen evolution reaction. *Nat. Mater*. **2016**, *15*, 197–203.

[4] Yang, D. X.; Zhu, Q. G.; Han, B. X. Electroreduction of CO_2 in ionic liquid-based electrolytes. *Innovation* **2020**, *1*, 100016.

[5] Liu, T. Y.; Diao, P. Nickel foam supported Cr-doped $NiCo_2O_4$/FeOOH nanoneedle arrays as a high-performance bifunctional electrocatalyst for overall water splitting. *Nano Res*. **2020**, *13*, 3299–3309.

[6] Shi, Y. M.; Zhang, B. Recent advances in transition metal phosphide nanomaterials: Synthesis and applications in hydrogen evolution reaction. *Chem. Soc. Rev*. **2016**, *45*, 1529–1541.

[7] Willinger, E.; Massué, C.; Schlögl, R.; Willinger, M. G. Identifying key structural features of IrO_x water splitting catalysts. *J. Am. Chem. Soc*. **2017**, *139*, 12093–12101.

[8] Walter, M. G.; Warren, E. L.; McKone, J. R.; Boettcher, S. W.; Mi, Q. X.; Santori, E. A.; Lewis, N. S. Solar water splitting cells. *Chem. Rev*. **2010**, *110*, 6446–6473.

[9] Xue, H. Y.; Zhang, H. Q.; Fricke, S.; Lüther, M.; Yang, Z. J.; Meng, A. L.; Bremser, W.; Li, Z. J. Scalable and energy-efficient synthesis of Co_xP for overall water splitting in alkaline media by high energy ball milling. *Sustainable Energy Fuels* **2020**, *4*, 1723–1729.

[10] Tang, C.; Zhang, R.; Lu, W. B.; He, L. B.; Jiang, X. E.; Asiri, A. M.; Sun, X. P. Fe-Doped CoP nanoarray: A monolithic multifunctional catalyst for highly efficient hydrogen generation. *Adv. Mater*. **2017**, *29*, 1602441.

[11] Liu, T. T.,; Ma, X.; Liu, D. N.; Hao, S.; Du, G.; Ma, Y. J.; Asiri, A. M.; Sun, X. P.; Chen, L. Mn doping of CoP nanosheets array: An efficient electrocatalyst for hydrogen evolution reaction with enhanced activity at all pH values. *ACS Catal*. **2017**, *7*, 98–102.

[12] Shi, J. H.; Qiu, F.; Yuan, W. B.; Guo, M. M.; Lu, Z. H. Nitrogen-doped carbon-decorated yolk-shell CoP@FeCoP micro-polyhedra derived from MOF for efficient overall water splitting. *Chem. Eng. J*. **2021**, *403*, 126312.

[13] Zhang, R.; Tang, C.; Kong, R. M.; Du, G.; Asiri, A. M.; Chen, L.; Sun, X. P. Al-doped CoP nanoarray: A durable water-splitting electrocatalyst with superhigh activity. *Nanoscale* **2017**, *9*, 4793–4800.

[14] Li, X. M.; Li, S. S.; Yoshida, A.; Sirisomboonchai, S.; Tang, K. Y.; Zuo, Z. J.; Hao, X. G.; Abudula, A.; Guan, G. Q. Mn doped CoP nanoparticle clusters: An efficient electrocatalyst for hydrogen evolution reaction. *Catal. Sci. Technol*. **2018**, *8*, 4407–4412.

[15] Gao, W.; Yan, M.; Cheung, H. Y.; Xi, Z. M.; Zhou, X. M.; Qin, Y. B.; Wong, C. Y.; Ho, J. C.; Chang, C. R.; Qu, Y. Q. Modulating electronic structure of CoP electrocatalysts towards enhanced hydrogen evolution by Ce chemical doping in both acidic and basic media. *Nano Energy* **2017**, *38*, 290–296.

[16] Cao, L. M.; Hu, Y. W.; Tang, S. F.; Iljin, A.; Wang, J. W.; Zhang, Z. M.; Lu, T. B. Fe-CoP electrocatalyst derived from a bimetallic Prussian blue analogue for large-current-density oxygen evolution and overall water splitting. *Adv. Sci*. **2018**, *5*, 1800949.

[17] Hu, G. J.; Xiang, J. X.; Li, J.; Liu, P.; Ali, R. N.; Xiang, B. Urchin-like ternary cobalt phosphosulfide as high-efficiency and stable bifunctional electrocatalyst for overall water splitting. *J. Catal*. **2019**, *371*, 126–134.

[18] Lou, X. W.; Archer, L. A.; Yang, Z. C. Hollow micro-/nanostructures: Synthesis and applications. *Adv. Mater*. **2008**, *20*, 3987–4019.

[19] Ren, Z. G.; Ren, X. C.; Zhang, L.; Fu, C. H.; Li, X. F.; Zhang, Y. X.; Gao, B.; Yang, L. J.; Chu, P. K.; Huo, K. F. Tungsten-doped CoP nanoneedle arrays grown on carbon cloth as efficient bifunctional electrocatalysts for overall water splitting. *ChemElectroChem* **2019**, *6*, 5229–5236.

[20] Ji, L. L.; Wang, J. Y.; Teng, X.; Meyer, T. J.; Chen, Z. F. CoP nanoframes as bifunctional electrocatalysts for efficient overall water splitting. *ACS Catal*. **2020**, *10*, 412–419.

[21] Liu, J. L.; Gao, Y.; Tang, X. X.; Zhan, K.; Zhao, B.; Xia, B. Y.; Yan, Y. Metal–organic framework-derived hierarchical ultrathin CoP nanosheets for overall water splitting. *J. Mater. Chem. A* **2020**, *8*, 19254–19261.

[22] Zhu, W. X.; Zhang, R.; Qu, F. L.; Asiri, A. M.; Sun, X. P. Design and application of foams for electrocatalysis. *ChemCatChem* **2017**, *9*, 1721–1743.
[23] Hou, J. G.; Sun, Y. Q.; Li, Z. W.; Zhang, B.; Cao, S. Y.; Wu, Y. Z.; Gao, Z. M.; Sun, L. C. Electrical behavior and electron transfer modulation of nickel–copper nanoalloys confined in nickel–copper nitrides nanowires array encapsulated in nitrogen-doped carbon framework as robust bifunctional electrocatalyst for overall water splitting. *Adv. Funct. Mater.* **2018**, *28*, 1803278.
[24] Cao, S.; You, N.; Wei, L.; Huang, C.; Fan, X. M.; Shi, K.; Yang, Z. H.; Zhang, W. X. CoP microscale prism-like superstructure arrays on Ni foam as an efficient bifunctional electrocatalyst for overall water splitting. *Inorg. Chem.* **2020**, *59*, 8522–8531.
[25] Yuan, W. Y.; Wang, X. Y.; Zhong, X. L.; Li, C. M. CoP nanoparticles *in situ* grown in three-dimensional hierarchical nanoporous carbons as superior electrocatalysts for hydrogen evolution. *ACS Appl. Mater. Interfaces* **2016**, *8*, 20720–20729.
[26] Qin, J. F.; Lin, J. H.; Chen, T. S.; Liu, D. P.; Xie, J. Y.; Guo, B. Y.; Wang, L.; Chai, Y. M.; Dong, B. Facile synthesis of V-doped CoP nanoparticles as bifunctional electrocatalyst for efficient water splitting. *J. Energy Chem.* **2019**, *39*, 182–187.
[27] Huang, Z. P.; Chen, Z. Z.; Chen, C. B.; Lv, C. C; Humphrey, M. G.; Zhang, C. Cobalt phosphide nanorods as an efficient electrocatalyst for the hydrogen evolution reaction. *Nano Energy* **2014**, *9*, 373–382.
[28] Li, W. J.; Yang, Q. R.; Chou, S. L.; Wang, J. Z.; Liu, H. K. Cobalt phosphide as a new anode material for sodium storage. *J. Power Sources* **2015**, *294*, 627–632.
[29] Suo, N.; Han, X. Q.; Chen, C.; He, X, Q.; Dou, Z. Y.; Lin, Z. H.; Cui, L. L.; Xiang, J. B. Engineering vanadium phosphide by iron doping as bifunctional electrocatalyst for overall water splitting. *Electrochim. Acta* **2020**, *333*, 135531.
[30] Wen, L. L.; Yu, J.; Xing, C. C.; Liu, D. L.; Lyu, X. J.; Cai, W. P.; Li, X. Y. Flexible vanadium-doped Ni_2P nanosheet arrays grown on carbon cloth for an efficient hydrogen evolution reaction. *Nanoscale* **2019**, *11*, 4198–4203.
[31] Chen, D.; Lu, R. H.; Pu, Z. H.; Zhu, J. W.; Li, H. W.; Liu, F.; Hu, S.; Luo, X.; Wu, J. S.; Zhao, Y. et al. Ru-doped 3D flower-like bimetallic phosphide with a climbing effect on overall water splitting. *Appl. Catal. B: Environ.* **2020**, *279*, 119396.
[32] Li, Y. J.; Mao, Z. F.; Wang, Q.; Li, D. B.; Wang, R.; He, B. B.; Gong, Y. S.; Wang, H. W. Hollow nanosheet array of phosphorus-anion-decorated cobalt disulfide as an efficient electrocatalyst for overall water splitting. *Chem. Eng. J.* **2020**, *390*, 124556.
[33] Zhang, S. G.; Gao, G. H.; Zhu, H.; Cai, L. J.; Jiang, X. D.; Lu, S. L.; Duan, F.; Dong, W. F.; Chai, Y.; Du, M. L. *In situ* interfacial engineering of nickel tungsten carbide Janus structures for highly efficient overall water splitting. *Sci. Bull.* **2020**, *65*, 640–650.
[34] Zhang, Y.; Guo, H. R.; Li, X. P.; Du, J.; Ren, W. L.; Song, R. A 3D multi-interface structure of coral-like Fe-Mo-S/Ni_3S_2@NF using for high-efficiency and stable overall water splitting. *Chem. Eng. J.* **2021**, *404*, 126483.
[35] Lim, J. W.; Jung, J. W.; Kim, N. Y.; Lee, G. Y.; Lee, H. J.; Lee, Y. H.; Choi, D. S.; Yoon, K. R.; Kim, Y. H.; Kim, I. D. et al. N_2-dopant of graphene with electrochemically switchable bifunctional ORR/OER catalysis for Zn-air battery. *Energy Storage Mater.* **2020**, *32*, 517–524.